The spherulitic and lamellar morphology of melt-crystallized isotactic polypropylene

D. R. Norton and A. Keller
H. H. Wills Physics Laboratory, University of Bristol, Tyndall Avenue, Bristol BS8 1TL, UK
(Received 25 May 1984; revised 24 October 1984)

A study is presented concerning the basic morphology of melt-crystallized isotactic polypropylene (iPP). Involved within, is the coordinated application of optical and electronmicroscopy on a range of commercial iPP-s, crystallized in the temperature range 100°C–150°C. For electron microscopy in particular, the permanganic etching technique has been used throughout, providing the simultaneous combination of both real space microstructures with electron diffraction information. The investigation itself has centred on the five different spherulite types, as identified optically, which were then correlated with the details of their particular lamellar morphology. It was found that each spherulite type is characterized by virtue of the arrangement of its constituent lamellae, in terms of orientation, habit type and crystal structure. Thus, specific correlations were obtained between the structural entities on all scales of the structure hierarchy.

(Keywords: polypropylene; morphology; crystallization; microstructure; electron microscopy)

INTRODUCTION

The crystalline architecture of isotactic polypropylene (iPP) is complex and multifaceted. This is manifest on different levels of the structural hierarchy. On the largest scale, i.e. on the level of the polarizing microscope, there exists a variety of spherulite types classified by their appearance between crossed polaroids, including sign and nature of birefringence. At the other extreme, on that of the crystal lattice, we have a muliplicity of polymorphs, distinguished by the mutual arrangement of the chains of otherwise identical conformation (all 3_1 helices as far as we know). On the intermediate level there are the lamellar structures, which, in the case of iPP can be of differing type both as regards the nature of the lamellae and their mutual arrangement. Further, and most intriguingly, there appears to be an interrelation between this structural multiplicity on the three distinct dimensional levels, a point being brought out strongly by the results of the present work. The objective of the work is to examine the structural variants on the three different levels and establish correlations such as exist between them, and thus remove a presently existing blockage to a fuller understanding of polypropylene structures. The strongest emphasis is on the level of the lamellae which represents the weakest link in our knowledge, particularly in bulk material.

Crystal structure

The conventional, and most widely occurring, crystal structure of polypropylene is the one determined first, by Natta and Corradini[1] with a monoclinic lattice, referred to later, when other polymorphs became recognized, as the 'α' structure. Soon after, a polymorph with a hexagonal lattice, the hexagonal or β structure, was recognized[2–5]. This structure only occurs occasionally, and even then only as a minority constituent of the bulk sample. Following this an even rarer third polymorph, based on a tricclinic lattice, the so-called 'γ' structure, was identified by Turner-Jones *et al.*[3]. Subsequent workers found, that the formation of this γ structure is promoted by hydrostatic pressure[6–8]. There is mention of a further structure, termed δ, found in polypropylenes with a high percentage of amorphous material[9]. In all these structures ($\alpha,\beta,\gamma,\delta$) the chain conformation is identical and corresponds to the familiar threefold (3_1) helix, the different polymorphs being distinct through different stacking geometries of these helices. In the present work the α and β structures will play a major part. The γ structure was observed by us and will be mentioned, even if it will have no significant role for the points we are to make, (although it does so in at least one, somewhat speculative, scheme featuring in the literature[10].

Spherulites

Padden and Keith[11] using thin films crystallized in the temperature range 110°C–148°C observed a variety of spherulitic appearances which they classified as representing four distinct types: I–IV. Types I and II, in addition to being formed within different temperature ranges, *Table 1*, have been defined by differences in their respective birefringence values: positive for the former and negative for the latter. Rarer types of spherulite, named III and IV, occur sporadically and appear to form within certain constraints of isothermal crystallization temperature (T_c); again see *Table 1*. They are characterized by a strong negative birefringence. As such, these types are easily distinguished optically, appearing highly luminous amidst a sea of much less bright spherulites. Numerous later studies[2,11,12] have shown that Types I and II crystallize with the monoclinic, α, crystal structure whilst Types III to IV crystallize with the hexagonal 'β' structure[2–5]. Another consideration distinguishing the two

0032-3861/85/050704-13$03.00

Table 1 Characteristics of spherulite types (previous study ref. 1)

Spherulite type	I	Mixed	II	III	IV
	Monoclinic			Hexagonal	
Crystal structure	α	α	α	β	β
Magnitude of birefringence (Δn)	~0.003	±0.002	0.002	0.007	0.007
Sign of birefringence	+ve	+ve/−ve	−ve	−ve	−ve
Concentric banding	No	No	No	No	Yes
Isothermal temperature of crystallization	<134° C	134° C–138° C	>138° C	<122° C	126° C–132° C

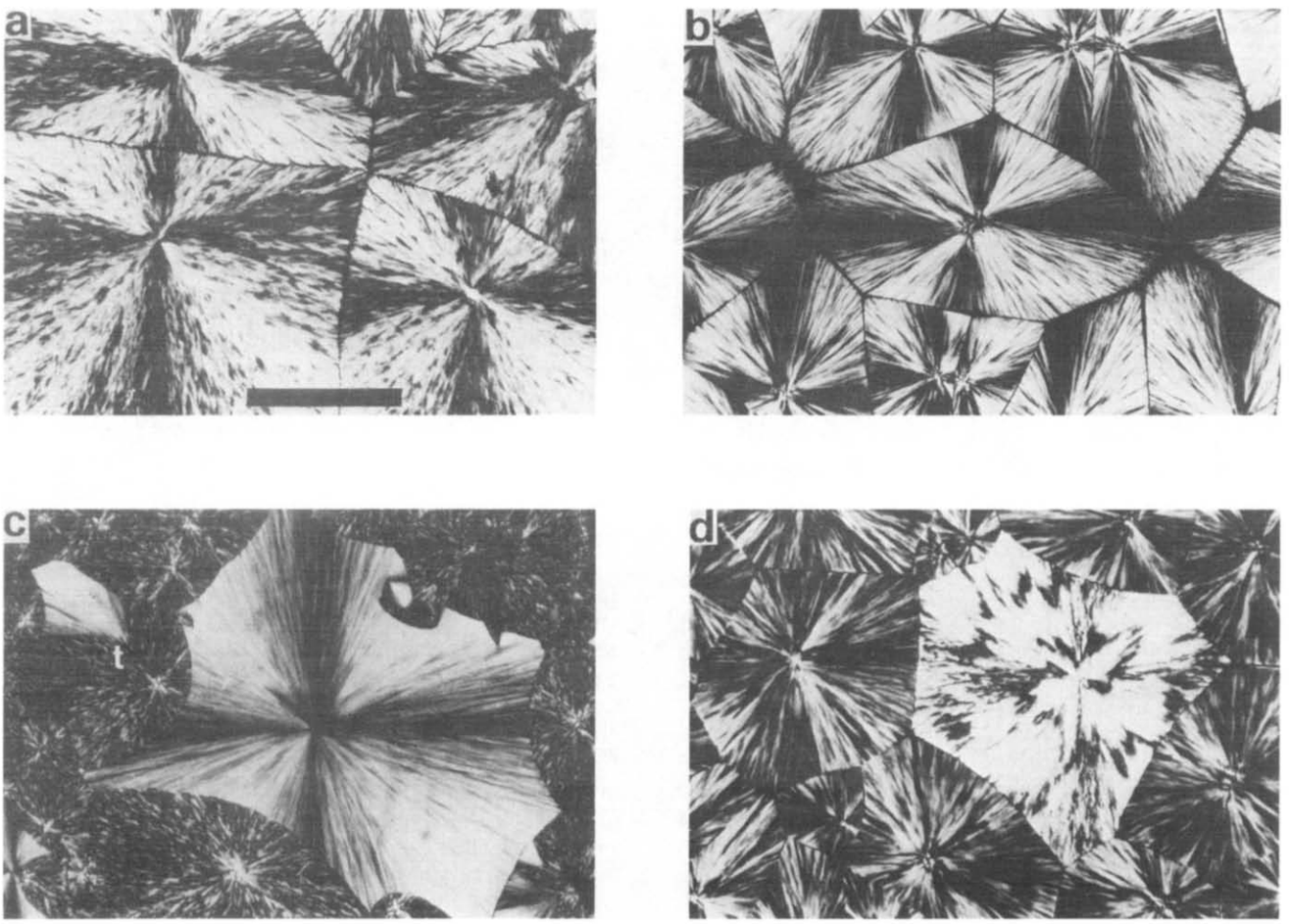

Figure 1 Different spherulite types, I–IV viewed in polarized light. Scale bar=200 μm. a, type I T_c=128°C; b, type II T_c=138°C; c, type III T_c=125°C; d, type IV T_c=130°C. Note also the $\alpha \rightarrow \beta$ transformation in the mixed spherulites of *Figure 1c*

crystal forms relates to the crystallization kinetics. It has been found that the respective rates of nucleation and growth vary for the two crystal phases, hence for the corresponding spherulites, quite considerably. Thus, Types III and IV nucleate at a much lower rate than Types I and II, but once nucleated they grow faster by between 20–70%[13]. These two opposing trends have the consequence that Types III and IV appear with noticeable frequency only below certain crystallization temperatures[11].

Intriguingly, the spherulites of most bulk crystallized samples belong to none of the above types, and occur as the so-called 'Mixed' spherulite type. These spherulites exhibit random distributions of positively and negatively birefringent regions where the birefringence, which although usually not measurable, is of low value. Correspondingly the unit cell of all spherulites falling into the mixed category is the monoclinic, α, variety. For this reason Types I, II and Mixed forms are often collectively referred to as α spherulites; similarly Types III and IV are often collectively denoted as β spherulites. The defining properties of all the spherulites, as perceived by previous studies, mainly ref. 11, are given in *Table 1*. Examples of all these spherulite types, as ensuing from the present work are illustrated by *Figures 1* and *2*. The temperatures quoted are those obtained for the nucleation of the different types under conditions of isothermal crystallization. The measurements were made on thin films and are not to be treated as rigorously defineable limits.

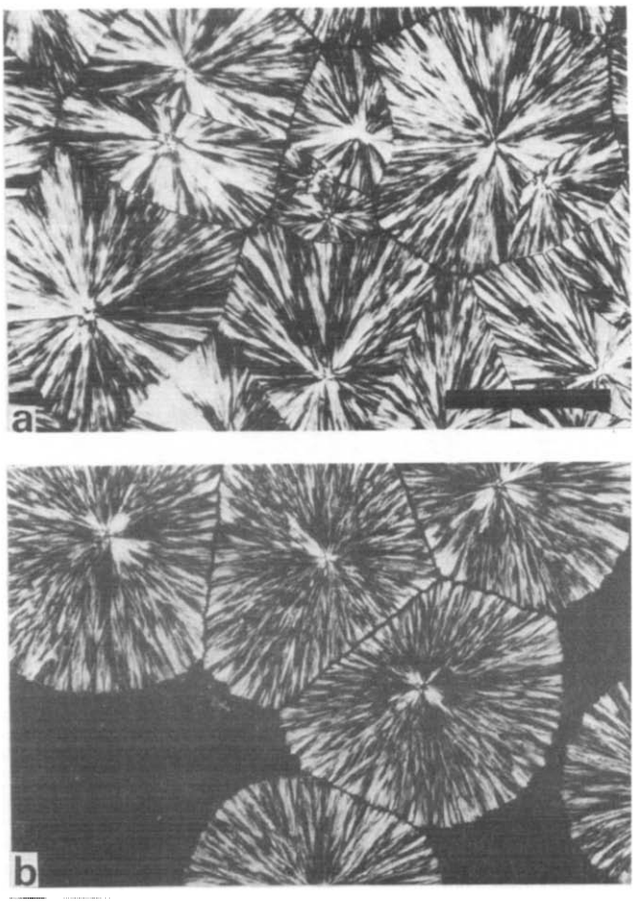

Figure 2 Two examples of the mixed variety of spherulite. Scale bar=100 μm. a, T_c=130°C; b, T_c=138°C (note centres which are positively birefringent)

Lamellae

The morphology on the resolution level of the electron-microscope is also complex. It is also somewhat unique, for the α-phase crystallizes both from solution[14,15] and the melt[10,16–18] as a three dimensional array of nearly orthogonal 'cross-hatched' lamellar arrangement. Solution studies have shown the basic structural unit to be a lath-like chain-folded lamellar crystal, these crystals forming relatively open networks in solution grown aggregates, but tightly interwoven structures in the melt. Evidence pertaining to the lamellar microstructure of β-phase material is scarce: an obvious consequence of the comparative rarity of this crystal form. The lamellae, such as claimed to be identified, are thought to exist as smooth stacks and sheets[12,16,19] similar to the known lamellar morphologies of more 'conventional' polymers. A detailed morphological analysis of the microstructures however, has been conspicuously absent. There are no direct morphological studies involving the γ-phase, even though it has been hypothesized in at least one work[10] that traces of it may have a role to play in the creation of the complex, mutually orthogonal lath assemblies arising in the α-form.

The general objective of the present work has already been stated. The more explicit subject is the examination of the relation between the variety of spherulites and the underlying lamellar microtexture which has become possible through a new preparative microscropic technique. This is the permanganic etching technique of Bassett, Hodge and Olley[19–20], and adapted here for use with various commercial iPP-s. As will be apparent, the findings, which form part of a more extensive study[21], will reveal a connection between spherulite type and the lamellar architecture.

In addition, distinction by crystal structure will also be invoked and correlated with both polarizing microscopy and with the electronmicroscopic examination of the morphology. In this we were aided by an additional feature of our electronmicroscope technique involving the detachment of a thin layer whereby electron diffraction information has become available. This enables us to identify crystal structure type with lamellar morphology, also providing relationships between morphology and lattice orientation for a given crystal structure. As the interior of bulk polypropylene is notoriously inaccessible to morphological work, and as, in addition, polypropylene is especially prone to beam damage, the significance of the achievement of an informative combination of both objectives will be evident to all concerned with structure problems on iPP.

EXPERIMENTAL

All materials used are grades of commercial isotactic polypropylene (iPP), supplied by ICI, kindly provided by Dr D. Blundell, and designated as AiPP, BiPP and CiPP. All are homopolymers and were supplied in granule form; they differ principally in their value of molecular weight. Use was made also of an extracted, highly isotactic derivative, called here HiPP, and a sample that shall be called PiPP, which is a polymer produced by another polymerization process and consequently possesses a different molecular weight distribution. Some characteristics of the samples as made available to us are given in *Table 2*. The experimental procedures were as follows. For polarizing optical microscopy, an extemely simple but powerful experimental tool for rapid identification, thin film samples were prepared by two methods. In the first the iPP was fused between coverslip and glass slide on a Kofler hot bench and then rapidly transferred to a Mettler hot-stage, maintained at a selected temperature between 100°C–150°C, until completely crystallized. At higher temperatures crystallization occurs under a nitrogen atmosphere, to prevent the effects of thermal degradation. In the second method, test tubes containing iPP are placed in a vacuum oven at 230°C; the melt is then sealed and immersed in a silicone oil bath at a suitably selected isothermal crystallization temperature (T_c). This latter preparation requires the microtomy of thin (≃10 μm) samples to facilitate optical microscopy.

The birefringence of the spherulite, Δn, is defined as follows

$$\Delta n = n_r - n_t \qquad (1)$$

where n_r and n_t are the respective refractive indices along the radial and tangential directions of the spherulite.

Table 2 iPP characteristics

	MFI 10 kg at 190°C
AiPP	0.8
BiPP	18
CiPP	56
PiPP, HiPP	$\bar{M}_w = 5 \times 10^4$, $\bar{M}_n = 8.5 \times 10^3$

These values were obtained on a Zeiss Ultraphot polarizing microscope using an Ehringhaus compensator to measure path difference D in the knowledge of the sample thickness (t) (ascertained in various simple ways) through the relation

$$\Delta n = D/t \tag{2}$$

For a number of reasons appreciable experimental error could be involved in the precise absolute values of Δn. Most pertinent for the present purpose are the relative differences in Δn between the various spherulite types. These differences are recorded in the next section.

A relatively recent development in the field of morphological research studies has been the introduction of the permanganic etching technique, used primarily with polyolefins. Although the potential of the method when used with iPP has been very briefly demonstrated[19], to date, the published material has been mainly confined to polyethylene, for which a number of beautiful and revealing papers have been reported[19,20,22-24]. Although basic technique and mode of practice remains similar for the present study a number of beneficial preparative modifications have been applied which justify a brief description.

Surfaces to be etched can take the form of the microtomed bulk or the surface of thin films (*ca.* 10–100 μm thick), similar in fact to the translucent specimens as used for optical microscopy. The technique has proved so successful that large areas, in some cases up to 1 cm^2, can be satisfactorily replicated. The major advancement has centred on the chemical nature of the etch. A less severe treatment is now preferred, where mixing sulphuric acid (H_2SO_4), with orthophosphoric acid (H_3PO_4) the purpose of which is to minimize the occurrence of artefacts[23], has proved particularly useful in the case of iPP. This arises from the fact that the molecular chemistry of iPP is rather too susceptible to the reagent used in the original recipe[25], as applied to polyethylene. While there are variations a 'typical treatment' is described below.

A managably sized surface is placed in a sealable test tube containing a 60:40 mixture of H_3PO_4 and H_2SO_4 with approximately 1/2% (wt%) potassium permanganate ($KMnO_4$). Etching takes place with the test tube supported in a small ultrasonic bath. Good results occur with etch times varying from 15 min to 5 h; 1 h usually being sufficient. After the desired treatment the following five stage cleansing recipe is recommended. Wash the specimen in a dilute solution of H_2O:H_2SO_4, clean in hydrogen peroxide, wash in distilled water, clean in acetone and finally dry in a vacuum oven for about 1 h at around 40°C. The etched and cleaned specimens are immediately replicated, after shadowing first with a very thin platinum/palladium (Pt/Pd) layer at an angle of 20–40°. A thicker and vertical backing of carbon follows. The Pt/Pd–C layer is removed by using a small blob of aqueous polyacrylic acid (PAA), which, when dry, can be prized away quite easily using a razor blade. The composite Pt/Pd–C–PAA layer is placed in distilled water, and after a sufficient time to allow for the PAA to dissolve ($\simeq$2 h), the replica is mounted on a grid for transmission electron microscopy (TEM).

During certain preparations a thin and irregular amount of iPP remains adhered to the replica surface. Rather than clean the replica, this detached polymer has proved to be very suitable for the pursuance of diffraction studies as mentioned above. Examination by TEM was performed using a Philips EM300, EM301 or JEOL 100CX, all equipped with a eucentric goniometer (±60°) and a nitrogen cold stage if necessary.

RESULTS

An optical classification of the spherulite types

The experiments produced a profusion of spherulitic forms where all the microstructures could be classified by the previously laid out categories, i.e. types I to IV and a Mixed form as described in the introduction. The experiments surveyed an arbitrarily chosen series of crystallization temperatures (T_c) in the range 100°C–150°C. Illustrations of the more prominent spherulite types are shown in *Figures 1a–d*, and *Figures 2a, b*, whilst the overall characteristics distinguishing each type is given in *Table 3;* (compare with existing data, *Table 1*). The more pertinent features relating to each spherulite type are described below.

Pure type I spherulites, (by 'pure' we mean types exhibiting a uniform Maltese Cross without additional extinction phenomena elsewhere), tend to be formed in thin films at $T_c \leqslant 136$°C, *Figure 1a*, (Sample HiPP, though, produced this spherulite type for T_c up to 140°C). The measured birefringence (Δn) is positive and shows slight variations in magnitude 0.004 to 0.001. The higher values are associated with the lower temperatures of crystallization. Pure type II spherulites, *Figure 1b*, are most usually found at temperatures greater than $T_c = 136$°C: this varies somewhat between specimens. For instance in sample HiPP this type only occurs prominently at $T_c \geqslant 138$°C. The actual temperature values

Table 3 Characteristics of spherulite types (present study)

Spherulite type	I	Mixed	II	III	IV
	Monoclinic			Hexagonal	
Crystal structure	α	α	α	β	β
Magnitude of birefringence (Δn)	0.001→ −0.004	≃ ± 0→ 0.003	−0.002→ −0.01	−0.007→ −0.014	0.007→ −0.016
Sign of birefringence	+ve	+ve/−ve	−ve	−ve	−ve
Concentric banding	No	No	No	No	Yes
Isothermal temperature of crystallization (T_c)	⩽137°C (in thin films) ⩽142°C (in HiPP)	up to ≃ 140° C	⩾136°C	⩽142°C	128° C–132° C

should not be regarded as rigid constraints, but rather, representing trends. Examples can be found where Types I and II exist simultaneously in the same sample. Type II spherulites are negative in biregringence, but the value is variable with quite disparate extremes; typically in the range $\Delta n_{min} = -0.002$ to $\Delta n_{max} = -0.01$. The high negative values correspond to high T_c.

The two monoclinic structures cited above will be said to be atypical of most specimens crystallized at $T_c \leqslant 140°C$. By far the overwhelming proportion of spherulites are termed 'Mixed', in that they possess no Maltese Cross, and are revealed as a radiating array of intermingled areas of positive/zero/negative birefringence, *Figure 2a*. This optical texture as regards coarseness and compactness can very significantly, imparting large differences in optical appearance. The partially mixed spherulites of *Figure 2a*, where the mixing is on a coarse scale allowing a ready resolution of the components, are biased toward an overall positive birefringence and occur at $T_c \leqslant 134°C$. The more finely mixed varieties, which are most common in the range $T_c = 132°C–140°C$, often do not permit clear resolution of the different regions, *Figure 2b*, and have very low and sometimes negligible birefringence. Even if here the fibrous structure is on a very fine scale a clear Maltese Cross is never apparent.

While the overall appearance of the mixed spherulites does not change on rotation of the stage, i.e. with respect to the polarizer and analyser direction, some variations could be seen on a fine scale of the individual dark lines. Although it was not easy to follow the behaviour of any particular dark line within the complex extinction pattern, it could be established that these variations amounted to azimuthal changes in position of approximately 10–30°, but no more. Namely, a given dark region was never observed to sweep around the full spherulite on a stage rotation while some of the dark regions stayed invariant to stage rotation altogether, the latter remaining dark on insertion of two crossed quarter wave plates at 45° to the analyser and polarizer direction. Similarly, some of the bright regions remained uncrossed by dark lines on stage rotation within a rotation range of up to 90°, retaining their overall negatively or positively birefringent character with the usual blue/orange colour test by sensitive tint plate (as defined with respect to the spherulite radius). Above about $T_c = 140°C$ the spherulites become again more coarsely fibrous but this time with a bias toward negative birefringence.

Spherulites termed Types III and IV, with an underlying hexagonal crystal structure, occur sporadically, and can be distinguished optically by high brightness within a less bright spherulitic background. Both types, III and IV, are characterized by a strong negative birefringence, *Figures 1c* and *1d*, and by a pronounced Maltese Cross. Type IV in addition also displays some concentric banding of a rather spiky, jagged character. Typical values for Δn vary, but are in the range -0.007 to -0.016; higher values are usually associated with Type IV spherulites. Often the birefringence can assume a very low value, in fact nearly zero, when the outline of the spherulitic boundary appears to contain a dark nonbirefringent structure. Sample CiPP of lowest molecular weight, when isothermally crystallized at around $T_c = 136°C$, produces an unusually high $\beta:\alpha$ spherulite type ratio, typically1:1. Fast cooling also promotes the growth of the β-phase. Any T_c below about 136°C will form some Type III spherulites, whilst temperatures between 124°C–132°C favour the type IV structure. Sample HiPP produced β-phase (Type III) at temperatures as high as $T_c = 142°C$.

A final point to be noticed in the case of α-spherulites is how the centres can display markedly different properties from the rest of the structure. This is evident in *Figure 2b*, where the centres show a high and positive Δn with the remainder of the spherulite texture a compact array of mixed fibres. The spherulites of *Figure 2b* were subsequently etched, *Figure 10*, to reveal the nature of this difference on the scale of the lamellae (see below).

For the electronmicroscopic examination a method was developed whereby the actual desired areas, as identified under the optical microscope, could be selected for the subsequent electron microscopy which was then pursued by the etching treatment described previously.

Lamellar morphologies

Monoclinic (α-form) spherulites. The unique and puzzling feature of cross-hatch type lamellar branching has been clearly identified to occur in all types of α-spherulites, (I, II and Mixed). *Figure 3b* illustrates how the branching affects the underlying lamellar morphology bestowing upon it what is essentially a bimodal orientation where radial lathlike lamellae nucleate tangential and 'cross-hatched' overgrowths of lamellae oriented nearly orthogonally. Khoury[15] proposed that this branching angle is 80°40′; this corresponds to parallelism of the *a* and *c* axes in one lattice with the *-c* and *-a* axes, respectively of the other. *Figure 3a*, shows the essential appearance and features of the 'cross-hatched' morphology. On this Figure the direction R represents the radial direction within the spherulite whilst the direction T represents the branched, tangential direction, characteristic of the cross-hatched overgrowth. The intercrossing and shorter lamellae, T. were measured to be at angles of around 80°C with respect to the radial direction, R.

Interestingly, and at such high temperatures (the specimen was crystallized at $T_c = 148°C$), differences in the respective thicknesses of the two components can be identified, the radial lamellae being slightly thicker: *ca.* 50 nm for the radial component and *ca.* 40 nm for the tangential component. The flat objects toward the top of *Figure 3b* represent a basal view of the radial lamellae, where in this portion of the spherulite misorientation has enabled a change of viewing direction. The likeness of the lamellae to the lath shaped solution grown crystals should be noted, when looking parallel to the molecular chain (*c*-axis).

The presentation of results will be facilitated by quoting the conclusions which have emerged from the observations. Accordingly it is the presence or absence of the nearly orthogonal component, variously called the 'cross-hatched' component or 'daughter' lamellae, which directly specifies the differences existing between all α-form spherulites. Types I and II, which are defined solely on the grounds of their birefringence, can be distinguished on the lamellar level by the relative ratio of the two components. For convenience let us assume that in the spherulite the lamellae are oriented either radially R or tangentially T as in *Figure 3a* (the two components of the

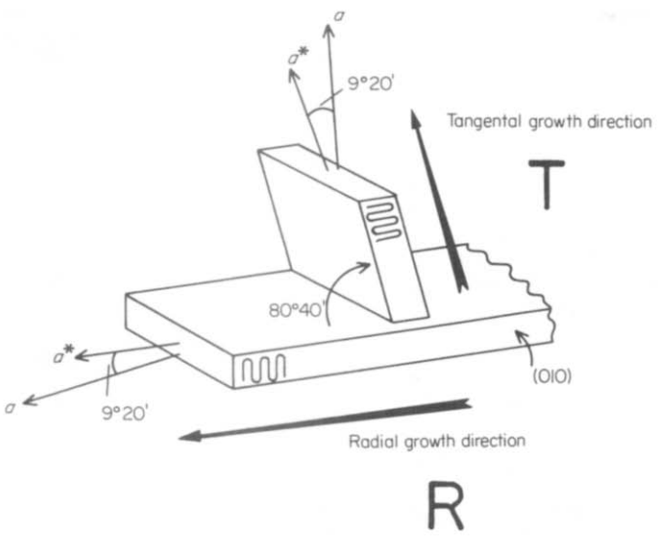

Figure 3 (a) Schematic representation of branching, indicating the epitaxial deposition of one branch. The 80° 40' branch angle corresponds to parallelism of the $\underline{a}$ and $\underline{c}$ axes of one lattice with the $-\underline{c}$ and $-\underline{a}$ axes respectively, of the other. (b) The general appearance of the 'cross-hatched' structure. The scale bar = 1 μm, R = spherulite radial direction, and T = tangential direction; with N = 'nodular' structures, T_c = 148°C

cross-hatching). It the molecular chains are closely normal to the lamellar surfaces, which by past precedents is the case for all lamellar structures, then radial and tangential lamellae on their own should display negative and positive birefringence respectively with respect to the radial direction in a spherulite (see discussion). It then ought to follow that in Type I spherulites the T and in the Type II spherulites the R lamellae should predominate. The above scheme was derived from a large number of micrographs and in what follows it will be illustrated by a few chosen examples.

The central sectional view of a Type I spherulite is shown in *Figure 4*. The specimen was crystallized at 'low' temperature, $T_c = 116$°C, and consequently the microstructure, for the most part, shows a complicated woven texture possessing a greater fraction of the tangentially oriented component. In numerous places the texture appears 'nodular', rather than lamellar. This is a common feature in many iPP morphologies, for example *Figure 3b*, marked N, and is thought to represent the earliest stages of branching. Progressing outward from the spherulite centre one sees increasing parallel and radially directed lamellae, although large areas are infilled with the tangential or nodular component.

Type II spherulites reveal a progressive reduction in the proportion of tangential lamellae with increasing temperature. The few chosen examples of *Figure 5a–d*, serve to illustrate this sequence. All are of sample HiPP and are taken at successively higher temperatures, $T_c = 135$°C, 140°C and 145°C respectively. They show how the overall fraction of the tangential component diminishes from a substantial amount, *Figure 5a*, to almost total absence in *Figure 5c* and *5d*. An additional interesting effect is depicted by these last two micrographs: the pictures, which represent an exaggerated stereoscopic pair, are related by a rotation of 72° about a NE–SW axis. Thus, it can easily be observed that the information regarding the spatial arrangement of the lamellae is dramatically modified upon tilting.

The sequence in *Figure 5a–d* is consistent with the observed birefringence which is becoming increasingly strongly negative for Type II spherulites formed at increasing T_c, verifying that it is the radial lamellae (R) which impart the negative character. Also noteworthy is the fact that in spherulites of essentially radial lamellae these lamellae can extend over virtually the full spherulite radius and are remarkably straight over long distances, *Figure 6*. (Here a lower T_c value is associated with the R $\gg$ T character, as compared to *Figure 5b*; a consequence of the different source of material involved).

The ubiquitous 'Mixed' spherulites are portrayed by one micrograph, *Figure 7*, taken at low magnification, which provides a link-up with the optical micrographs illustrating, amongst others, the complimentary nature of the two techniques. Mixed spherulites represent the more general case of monoclinic morphologies in that they possess areas of both positive and negative birefringence. On the lamellar scale this is merely the result of specific locations displaying a predominance of radial lamellae, which appear as pockets of negative birefringence under the polarizing microscope. Alternatively, there are regions of an exess of the tangential component, which would exhibit positive birefringence. Typical areas where these differences are present in *Figure 7* are marked R, F, and T respectively. (Regions marked F represent flat-on views of lamellae, they should display zero birefringence; see discussion section).

Hexagonal (β-form) spherulites. These comprise the type III and IV spherulites. The corresponding

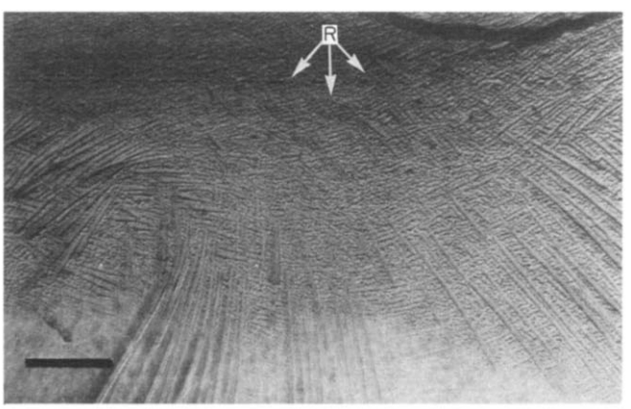

Figure 4 Lamellar texture in a type I spherulite, $T_c = 116$°C. The structure is an intimately woven array, with large amounts of 'cross-hatched' lamellae. The radial direction is indicated; the scale bar = 1/2 μm

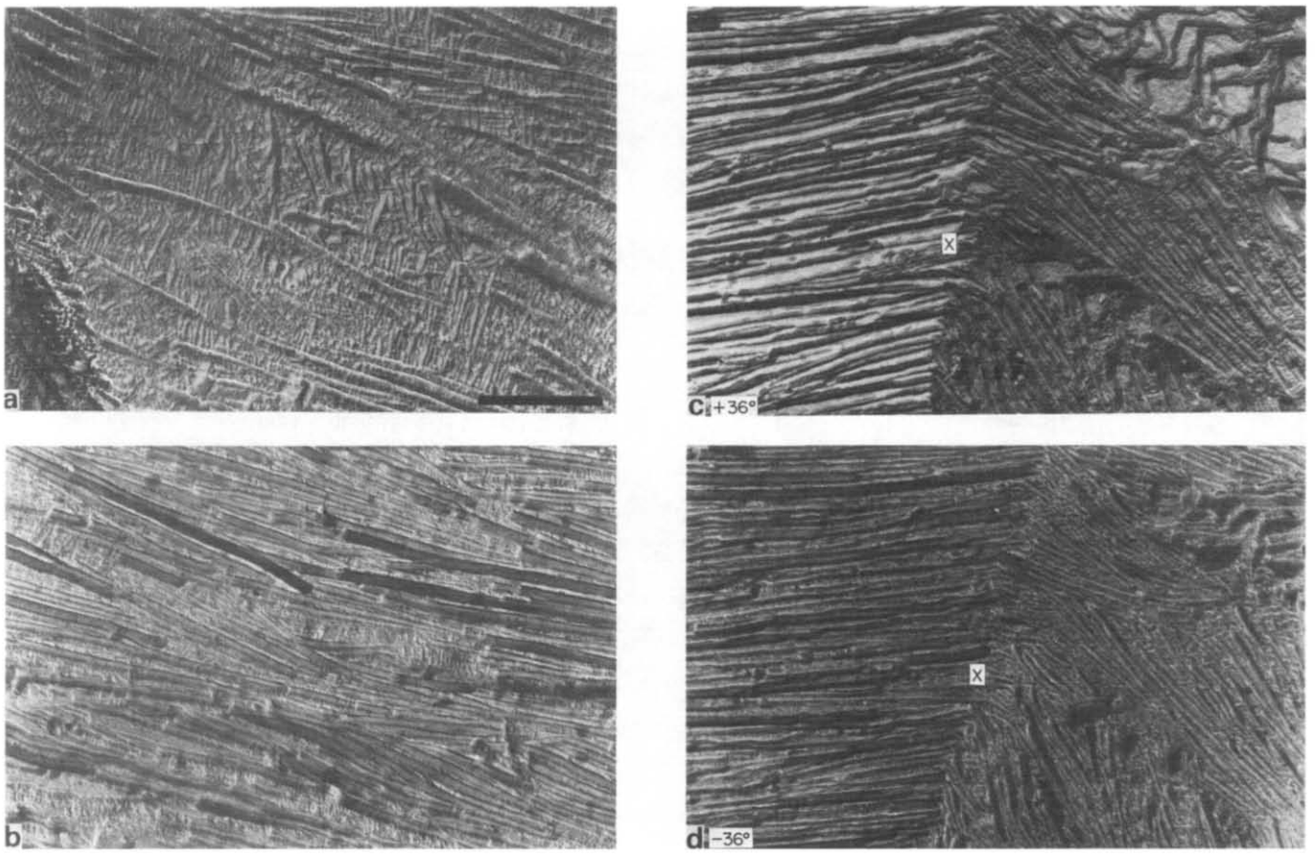

Figure 5 Three type II perspectives showing the disappearance of the tangential lamellae with increasing T_c. The scale bar=1 μm. a, T_c=135°C; b, T_c=140°C; c, T_c=145°C: +36° tilt; d, T_c=145°C: −36° tilt

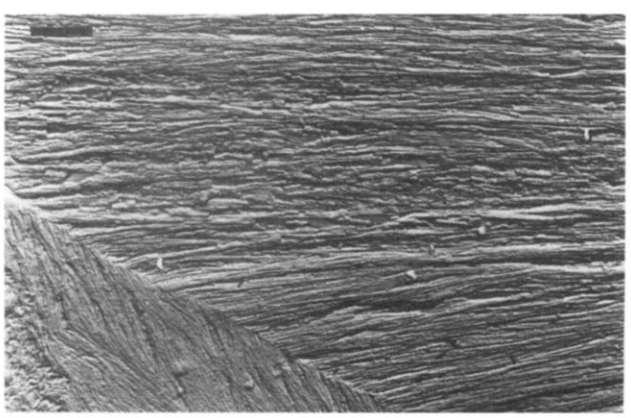

Figure 6 General appearance of the type II morphologies; very straight radial lamellae with only small amounts of tangential 'cross-hatch': T_c=136°C. Scale bar=3 μm

morphological observations on the lamellar level were amongst the most unambiguous and straightforward in the present study. They were found to consist of broad, locally parallel stacked lamellae, just as in the spherulites of other polymers. *Figure 8a* affords a low magnification view of the greater part of a Type III spherulite, where the replicated section passes through the spherulite diameter revealing the sheaf-like propagation of the space filling lamellae. Also clear is the flat-on view of lamellae within the lobes outside the sheaf centre. *Figure 8b* indicates these two perspectives revealed more fully at higher magnification. On the right-hand side, the lamellae are stacked parallel and edge-on, a typical *b*-axis profile,

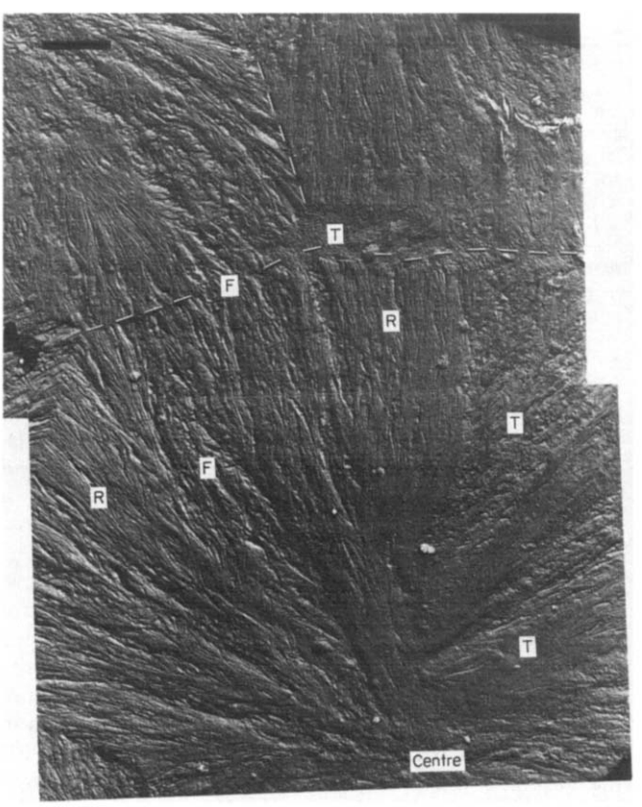

Figure 7 Low magnification of mixed type spherulite. The spherulite boundaries and centres are marked. Areas that appear to consist of predominantly radial (R) tangential (T) and flat-on (F) lamellae are indicated. T_c=130°C, scale bar=3 μm

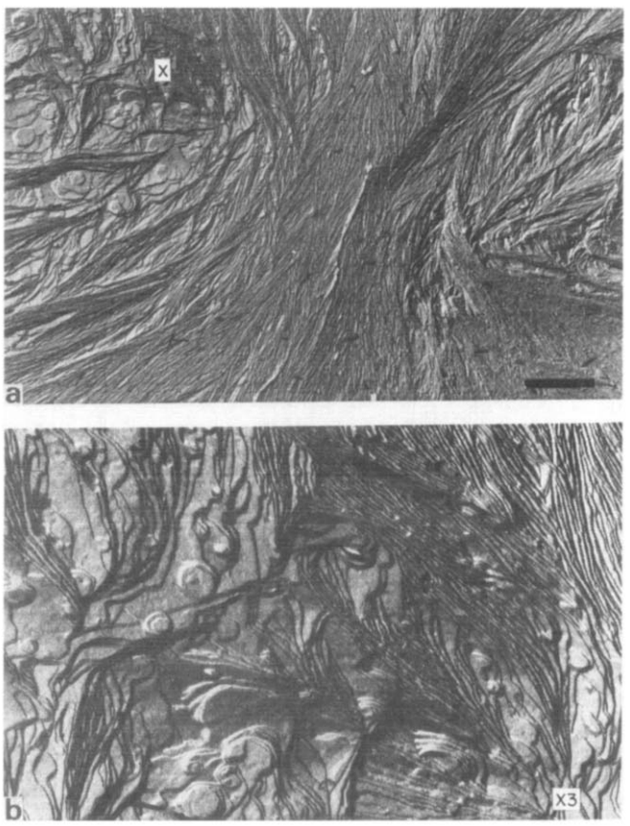

Figure 8 (a) Centre of a type III spherulite, showing smooth radiating lamellae and the sheaf-like nature of growth. Scale bar=3 μ, T_c=125°C. (b) Magnification of area X in *Figure 8a*

whilst the left-hand side illustrates the situation when the lamellae are viewed flat-on; i.e. closely along the *c*-axis, or molecular chain direction. The micrographs reveal that the lamellae are extended sheet structures in all lateral directions, rather than the lath-like entities as is the case for α-spherulites. Both Figures quite clearly show the development of numerous hexagonal etch terraces, indicating that possibly screw dislocation growth mechanisms are operative. Furthermore, in the flat-on view the lamellae may appear either rounded or faceted. In either case they tend to occur as elongated hexagons where the elongation is in the growth direction as referred to the spherulite. The right hand side of *Figure 9* shows the lamellar microtexture in the case of type IV spherulites. For this, the actual specimen of *Figure 1d* was treated for TEM work with the same α/β (Mixed/type IV) boundary readily identifiable in both optical and electron microscopy. The lamellae show a propensity to twist along the radial growth direction, thus presenting a broad spread or orientations varying from *b*-axis to *c*-axis profiles. The sequence of spherulite types just presented is characteristic of all isotactic polypropylenes. The exact temperature ranges of their formation (*Table 3*) and individual specific details are influenced by the degree of stereoregularity. Further work to be published will display such differences.

Electron diffraction. In the course of electron microscopy it was found that extraction replicas could be obtained from most types of specimen, which can be used to provide electron diffraction information. The polypropylene which adheres as a thin film, and in small quantities, is sufficient to provide electron diffraction patterns in the form of sharp spots and arcs. Three examples will briefly demonstrate the findings.

Figure 11 shows an area actually used to obtain a diffraction pattern; polymer which diffracts is revealed in dark contrast while the resulting pattern is shown by the inset. It can be indexed using the monoclinic structure of α-polypropylene (see *Figure 12*). It should be noticed that the lamellar orientation displayed by *Figure 11*, which is from a type II spherulite, is interpreted as a projection along (or near to) the radial growth direction. Hence the view is of a highly nondiametral spherulite section where lamellae are splaying out of the plane of the page. In contrast, in *Figure 12* the section is closely diametral. It is to be noted from *Figure 12* that the diffracting polymer adheres predominantly in one set of lamellar orientations

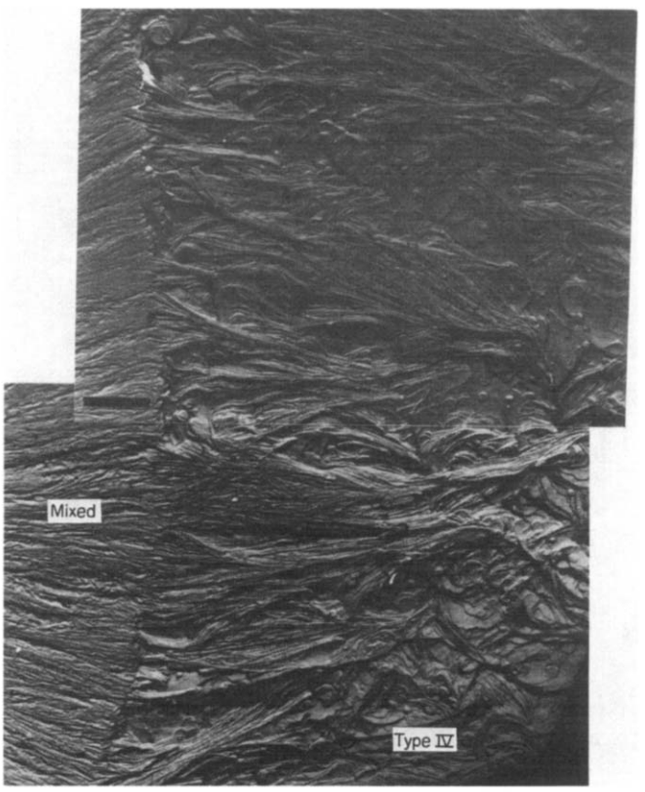

Figure 9 Spherulite boundary between type IV and mixed type microstructures. The actual spherulite is depicted in *Figure 1d*; scale bar=3 μm

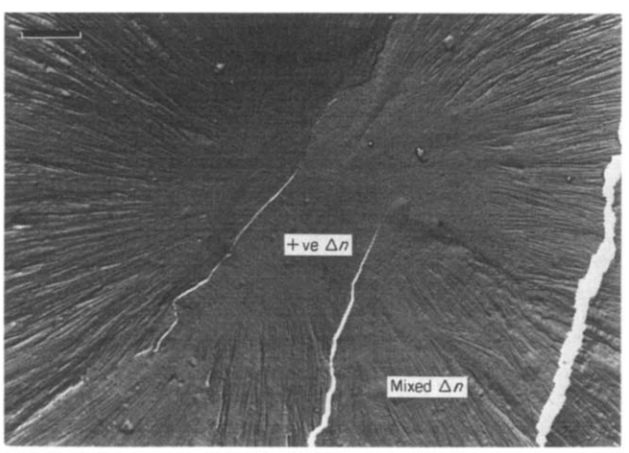

Figure 10 Centre of the spherulites of *Figure 2b*. Lamellar texture clearly varies in the central region. Scale bar=3 μm

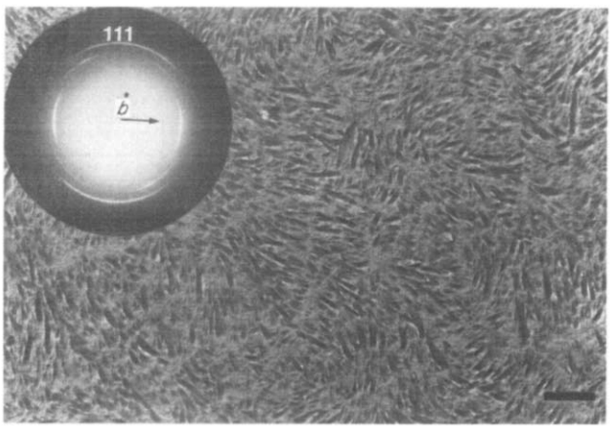

Figure 11 Typical extraction replica with α-form diffraction pattern. The latter is taken from the area to the right of the pattern. The diffracting polymer is revealed in dark contrast in a view which is predominantly parallel to the spherulite radius. Scale bar=1 μm

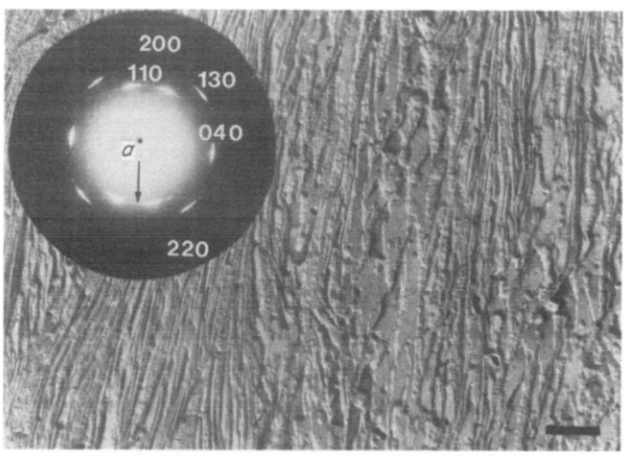

Figure 12 Detachement replica from a closely diametral section of an α spherulite with the corresponding diffraction pattern. The principal reflexions are *hk*0 of the α structure

namely, in the flat-on orientation, which in a cross-hatched structure comprises only portions of the R lamellae, but not the T lamellae. Thus, the technique discriminates between the two lamella types R and T, in favour of R, and so does, of course, the resulting diffraction pattern.

The indexed pattern of *Figure 12* could be said to be typical of all α-spherulites. The pattern consists of an inner set of slightly arced *hk*0 reflections, indicating that in most places the *c*-axis is largely perpendicular to this field of view. Frequently a few weak and diffuse reflections not belonging to the a^*b^* reciprocal lattice net are also imaged. Although these are usually the oblique 111 or 131 crystal planes from the α-phase, occasionally certain γ-phase (triclinic) reflections are apparent.

Figure 13 provides diffraction information on the other prominent iPP crystal structure, namely that of the hexagonal β-phase. Two prominent reflections occur at $d=5.5$ Å and $d=4.2$ Å. If the unit cell is assumed similar to that of other workers[4,5] then the reflecting planes correspond to 300 and 301, respectively, as indexed on a rhombohedral cell. In closely diametral sections one of the three equivalent {300} pairs dominates, the one normal to the radial growth direction (*Figure 14*).

DISCUSSION

It is now possible, and for the first time, to attempt a clarification of the complex, and often ambiguous, past classifications of polypropylene spherulites, in terms of their lamellar structures. The new development rests on a technical advance: a new electron microscopic sample preparation technique based upon a refinement of the permanganic etching method, providing clear 'real space' imaging of polypropylene microstructures. In the following discussion we will combine the birefringence and the newly observed features of the microstructure in a correlated morphological analysis.

Optical principles

For the interpretation and correlation of birefringence effects the following needs to be invoked. In iPP the direction of the molecular chain corresponds to that of maximum polarizability[26]. The corresponding crystal direction will therefore be the largest axis of the crystal indicatrix. In the hexagonal β-phase this indicatrix will be uniaxial and of positive character ($n_c > n_a = n_b$). The chain conformation (3_1 helix), hence polarizability along the chain direction, will be the same for the α crystal form, yet the packing of the chain will produce a monoclinic

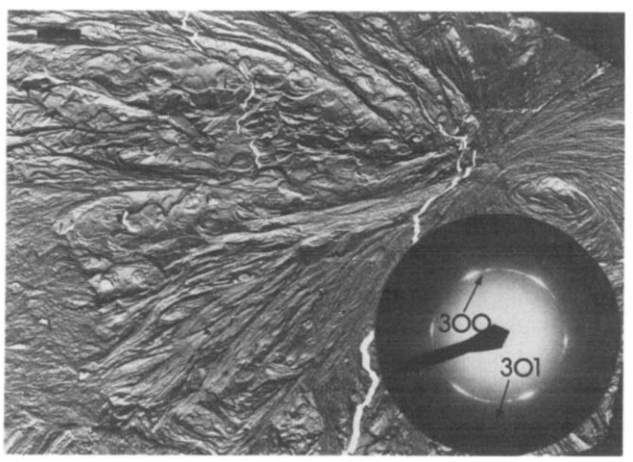

Figure 13 Typical hexagonal, β-spherulite and diffraction pattern; the diffracting area is top left of the micrograph. The scale bar=1 μm

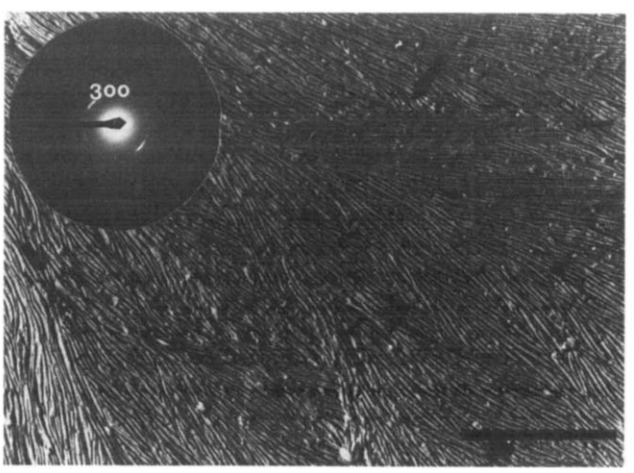

Figure 14 Lamellae in β-spherulite with corresponding diffraction pattern shown in inset. Pattern indicates the growth direction which is one of the hexagonal, ⟨300⟩ directions

symmetry. Because of this the optic indicatrix is, strictly speaking, biaxial. The biaxial character however, will be weak, ($n_a \simeq n_b$) hence to a good approximation we can consider all α crystals as positively uniaxial. It follows that, wherever the chain direction is tangential, with respect to the spherulite radius, the sign of the birefringence of the spherulite, Δn, will be negative. Conversely, whenever the chain direction is radial Δn will be positive. Where a combination of the two pertains the optic character of the spherulite will depend on which of the two orientations dominates. If the regions comprising each of the two dominant orientations are resolvable with visible light the spherulite is expected to display corresponding negatively and positively birefringent regions accordingly.

When relating lamellar microstructure to spherulite birefringence the important point to recall is the fact that the chain direction is close to normal to the lamellar surfaces (in iPP exactly so). Accordingly in iPP lamella will be represented by a uniaxial (or closely so) optic indicatrix of positive character with the optic axis parallel to the lamellar normal. All the combined birefringence and morphological observations made in this work follow from these simple statements. We shall take these in turn:

Correlation between spherulitic type and lamellar structure

β-spherulites. The simplest situation is presented by the hexagonal, β crystal structure based spherulites, types III and IV. These, as we have shown, consist of extended smooth lamellae growing radially outwards as in most other conventional polymer spherulites (*Figures 8,9,13,14*), hence the usual considerations for interpreting spherulite optics apply. Thus the lamellar normals, hence c axes, being tangential the observed negative sign of the birefringence follows. If all the orientations around the spherulite radius (with the c direction being tangential throughout) are averaged on the scale below the resolution by visible light a uniformly bright field will be seen accounting for the type III spherulites. If the optic axial direction changes periodically along the spherulite radius, while remaining normal to it, and the periodicity itself is within optical resolution, the familiar banded spherulites result, accounting for type IV. In terms of lamellae this means that we see the lamellae alternately flat-on and edge-on with all states in between. While the exact topology and space filling, not to speak of the origin, of this helicoidal type arrangement is still largely unknown, *Figure 9*, taken of type IV spherulite, is at least consistent with such a periodically varying lamellar orientation, particularly when the irregularity and jaggedness of the banding in the corresponding optical micrograph (*Figure 1d*) is taken into consideration. In any event the noticeable difference between the two spherulite types ('Mixed α' and type IV) juxtaposed in *Figure 9* should uphold any contention that the spherulite on the right hand side of *Figure 9* is as good a representation of the morphological equivalent of a roughly banded spherulite as can be expected.

The numerical values themselves deserve comment. Padden and Keith[11] measured Δn, for α crystal spherulites, to be approximately 0.007 ± 0.001, while Samuels[5] found a more complex development; for Type III spherulites the measured refractive indices were, $n_a = 1.496$ and $n_c = 1.507$ giving $\Delta n = -0.011$. For type IV spherulites $n_a = 1.496$ but n_c varied between 1.498 and 1.519, giving $\Delta n_{max} = -0.023$ and $\Delta n_{min} = -0.002$. In the current study observed Δn values fall in the range -0.007 to -0.016, in line with the previous works. As the β crystal form cannot be obtained as an oriented film, since tension transforms it into the α-form[3,9], there is no independent estimate of the intrinsic birefringence of the β-phase as such.

α-spherulites. As laid out in the Results section the situation in an α spherulite is influenced by the 'cross-hatching' phenomen, apparently unique to iPP. Of the two closely orthogonal components of the cross-hatch the radial R components (*Figure 3a*) on their own would give rise to negatively birefringent spherulites (as in the β spherulites above) while the tangential (T) lamellae would on their own create positive birefringence. As however, the latter occur in combination with the R lamellae their presence will reduce the negative birefringence due to the R lamellae, and if in sufficient abundance may impart their own sign making the spherulite itself positively birefringent. Accordingly, type I and type II spherulites should be distinguished by the presence and/or degree of cross-hatch. Thus without any cross-hatch the spherulite should be of type II. In the presence of cross-hatch it could be either I or II. There is no sharp morphologically distinct stage where the transition occurs. Rather it represents one stage in a continuously varying ratio of R and T lamellae, hence degree of cross-hatch, there being a stage where the birefringence due to R and T lamellae compensate and the spherulite will be nonbirefringent. In an ideal (for qualification see below) two dimensional (thin film) spherulite, or in a near diametral section of a three dimensional spherulite the positive contribution of the T lamella will always be the larger one, as the T lamellae will all be seen edge-on. This is in contrast to the R lamellae where the negative birefringence is due to an average effect of the edge-on and flat-on (and intermediate) views. Hence, under the usual conditions of observation the switch over from type II to type I spherulites will be observed at a stage where the T lamellae, still represent a minority component.

As will be apparent from the Results section the above expectations have been fully borne out by the observations: in particular, the predominantly (or exclusively) radial lamellar character of the type II spherulites (*Figure 6*) and the strongly cross-hatched character of the type I spherulite (*Figure 4*) revealing also the existence of a continuous gradation in the degree of cross hatch (*Figure 5*). The results reveal further that the degree of cross hatch increases with decreasing crystallization temperature (*Figure 5*).

The origin of the most common 'Mixed' spherulites has already been indicated in the Results section. They are the consequence of the inhomogeneity of the spherulite, where regions with predominantly R lamellae, such as giving negative birefringence, coexist with regions with sufficient amount of cross-hatch to produce positive birefringence within a given spherulite, each region being on a scale such as to be resolvable by visible light. Here the positively and negatively birefringent regions are delineated by extinguishing boundaries imparting an irregular fine structure to the spherulite as a whole as seen in the polarizing microscope. The large scale inhomogeneity within the 'Mixed' spherulites is clearly identifiable in low magnification electron micrographs (*Figure 7*), together with the corresponding

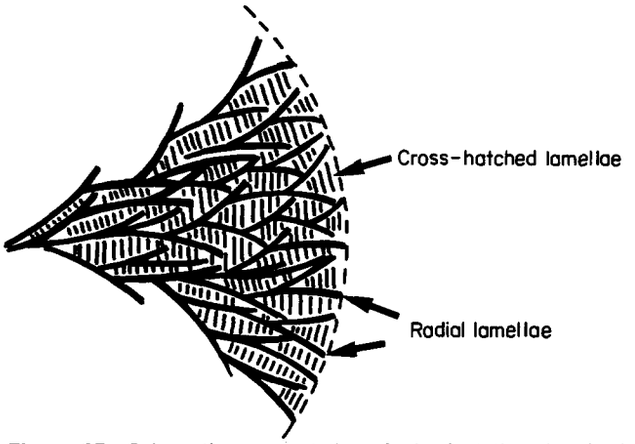

Figure 15 Schematic representation of misorientations in mixed spherulites. This would remove the maltese cross extinction and produce the complex extinguishing line patterns as observed in optical microscopy

predominantly radial or cross-hatched structures marked as R and T respectively. *Figure 7* also reveals that in regions with predominantly R type lamellae these lamellae can appear in flat-on view over extended areas (marked F). When large enough for optical viewing such regions will appear dark under the polarizing microscope.

Figure 2b represents a special case of inhomogeneity, where the central region is distinct and positively birefringent, becoming the usual 'Mixed' type further along the radius. On the lamellar scale the distinct central region is seen to have a more finely woven cross hatched structure consistent with the uniformly positively birefringent character, *Figure 10*.

At this point it may be useful to recall that optical extinction effects can be due to three sources: (a) Viewing is along an optic axis. This will arise when the lamellae are seen flat-on over optically resolvable regions. (b) Retardations due to components in mutually perpendicular orientation exactly compensate. This will arise for a particular ratio of R and T lamellae. (c) Transmission directions of the indicatrix coincide with extinction directions of polarizer and analyser. Effects (a) and (b) are invariant to stage rotation and correspond to actual zero birefringence. As such, they persist on viewing between additionally inserted crossed quarter wave plates. Effect (a) is the same as that which gives rise to concentric extinction bands in the corresponding β spherulites (type IV), while (b) is a consequence of the cross-hatching and is thus characteristic to the α-spherulites. Effect (c) is of altogether different origin and corresponds not to zero birefringence but to zero amplitude effect and its location moves with rotation of the microscope stage accordingly. Further, this extinction effect is absent when viewed between crossed quarter wave plates. The effect described as (c) is the source of the usual maltese cross present in all spherulites with the exception of the 'Mixed' variety. The 'Mixed' spherulites clearly evade the above classification. The absence of a clear maltese cross signifies that there must be departures from perfect spherical symmetry, at least on the local scale of the extinguishing line structure. The limited movements of the dark lines observed on rotations of up to $\sim 30°$ (but not more) indicates that there are misorientations of the optic indicatrix up to $\sim 30°$ with respect to the exact radial and/or tangential dispositions. Further, that within the angular interval of 0°–30° this orientation varies from one locality to the other when, say, following a radial path. A locally curving development of the dominant lamellae, such as in *Figure 15*, together with the corresponding undulations in orientation of the cross-hatched regions enclosed by them would account for the above cited observations. Indeed, electron micrographs such as *Figure 7* bear out the reality of this model. The variability of the degree of cross-hatching itself when passing from one locality to another would still remain responsible for the genuine variations of the sign of birefringence not obscured by the local and limited variation in orientation such as in *Figure 15*.

It needs adding that within spherulites grown in thin films the lamellae of either R or T kind have a greater propensity to grow edge-on, hence each will display their maximum contribution to the birefringence, as opposed to thicker samples or near diametral sections of the bulk where the R lamellae will have equal chance of being either viewed edge-on or flat-on with correspondingly reduced contributions to the mean birefringence. In the flat-on view of the R lamellae the T lamellae emanating from them are still seen edge-on and with our preparation method will now appear as mere stumps or blobs protruding outwards from the specimen plane (*Figure 3b*).

We may now turn to the actual numerical value of the birefringence for the α-spherulites. The intrinsic refractive indices have been calculated by a number of authors [27,28] while Wilchinsky[29] and Padden and Keith[11] observed Δn values for highly stretched films. Calculated values average $n_a = 1.512$, $n_c = 1.544$, hence $\Delta n_{max} = +0.032$.

In observed cases on stretched films the maximum value for Δn was between $+0.02$ and $+0.03$ depending upon crystallinity. For comparison with experiment we need to choose spherulites with as many chains oriented tangentially as possible, hence producing the maximum negative value for Δn. This will be realized by spherulite type II such as consist practically exclusively of R lamellae. Further, since the intrinsic refractive indices are, and should be, similar for the α and β forms we might expect closely similar birefringence values for the most birefringent type II and for type III spherulites. This in fact is the observed case where Δn for type II spherulites grown at high temperatures is approximately equal to Δn for β-phase spherulites, see *Table 3*. These are about 1/3–1/2 of the calculated values. In view of the randomisation around *a* the result seems highly reasonable.

We can now focus our attention to the observed differences between R and T lamellae other than their orientation. As already stated the R lamellae are definitely thicker than the T lamellae (especially so at high T_cs) *ca.* 50 nm vs. 40 nm. Consistent with this is the observed melting behaviour, for, if positive spherulites are taken to near their melt temperature they turn negative[11]. This suggests that the cross-hatching branches have melted leaving only a negative radial contribution to the spherulite birefringence. Both effects indicate that the T lamellae crystallized subsequently, possibly due to a segregation effect either by molecular weight or tacticity.

On the nature of the lamellae and origin of cross-hatch

Turning now to the problem of the causes of lamellar cross-hatching, most authors agree that some form of epitaxy is involved. Khoury[15], in a detailed study of solution grown aggregates, proposed the epitaxial growth of twinned branches with the lamellae forming an acute

angle of about 80° 40′ with the radial laths. Similar branch angles are found to exist for all spherulites studies here. The angle of branching requires the parallelism of the $\underline{a}$ and $\underline{c}$ axes of one lamella with the $-\underline{c}$ and $-\underline{a}$ axes, respectively of the other; the mismatch of the $\underline{a}$ and $\underline{c}$ lattice parameter is about 2.3%. Subsequently Padden and Keith[10] proposed that the cross-hatch is initiated at the lateral (010) edges of lamellae and involves the deposition of minute patches of γ-phase, triclinic, iPP. This gives a match between the $\underline{a}$ axis of the 'α' and the $\underline{c}$ axis of the 'γ' phases of around 0.6%. In another study by Clark and Spruiell[30], on the crystallization of melts during flow, another hypothesis was formulated: the expitaxial fit is between the separation (13.1 Å) of two chain folds in the primary lamellae (R lamellae in the present study), and the spacing between two turns of the iPP helix (13.0 Å). Finally, it should be noted that if the a^* axis is the growth direction, hence by implication the corresponding lateral axis of the lamellae, the lamellar fold surface is not (001), but rather a surface inclined at 9° 20′ to it (the difference between the $\underline{a}$ and a^* axes), i.e. $\bar{1}06$[18,30].

The evidence presented here appears to favour some form of 'pure' epitaxy, i.e. one that is related to some fundamental lattice constant, rather than a method of branch propagation by the deposition of an intermediate γ-phase. Three reasons for this can be quoted. (1) Extensive experiments with electron diffraction have produced only scarce evidence of γ-phase (some of which is present in most iPP-s in any case); (2) raising the temperature of crystallization, which should produce γ-phase segregation on a gross scale, and thus produce correspondingly larger fluctuations in the incidence of cross-hatching, does not appear to occur; (3) Above $T_c = 147$°C γ-phase transforms to α-phase, therefore at $T_c \geqslant 147$°C no γ-phase should be produced and subsequently little or no cross-hatching. However, *Figure 3b*, formed at $T_c = 148$°C indicates that this is not the case, as here large amounts of cross-hatching is self evident in a widespread and well developed form. A final consideration that may have some influence on the epitaxial nature of the cross-hatching is cited in the previous paragraph: namely the fact that the lamellar fold surface is not (001) but ($\bar{1}06$). This particular situation could require the development of (001)/(100) 'microfaceting' giving a jagged geometry to the fold surface on the scale of a few fold repeats; this in turn might promote the initiation of the cross-hatched lamellae.

It could be asked whether the cross-hatch develops concurrently with the radial growth of the spherulite or subsequently from material left uncrystallized during isothermal crystallization. While some cross-hatch formation due to the latter reason cannot be excluded it certainly does not influence the optical character of the spherulite: i.e. a positive spherulite is seen positive during isothermal growth at T_c. Hence the cross-hatch responsible for the positive character must already be present at that stage. Even so, perhaps some of the lower thickness cross-hatched lamellae observed in the negative spherulites formed at the highest temperatures may be due to segregation and subsequent crystallization at lower temperatures. More probably, the lower thicknesses are accounted for by a reduced isothermal thickening effect in that they formed at T_c but at a slightly later stage than their radial counterparts.

A comment on spherulite architecture

In broadest generality a spherulite can be defined as a crystal aggregate having spherical symmetry. Such a crystal aggregate arises by radial growth of crystals from a common centre. Such growth and the resulting spherically symmetrical end product, however, can arise in more than one way, most conveniently classified into two main categories.

In category 1 we have a central nucleating entity which initiates crystal growth in all directions. This is depicted by *Figure 16a*. Here the different crystals are nucleated separately and grow uncorrelated and remain so within the developing spherulite.

In category 2 the spherulite develops from one single crystal through essentially unidirectional growth (the source of nucleation of the initial crystal itself is of no consequence for the final spherulite). The spherical shape is attained through continuous branching and fanning via the intermediate stage of sheaves. The final spherical object (*Figure 16b*) has the following properties: First, each point within it and all along the growth front is in generic continuity with the central crystal which has initiated the growth. Secondly, the spherical symmetry does not extend to the central region, which preserves its sheaf-like features with a characteristic double circle or double leaf-like appearance, (as seen in two dimensional perspective, *Figure 16b*; in polymers the growing crystals are lamellae, which are most conspicuous in edge on view, where they appear as if they were fibres.) In much of the literature the term spherulite is reserved to this category 2.

The above classification is clearly relevant to the present observations on iPP spherulites in a rather unique manner. The β spherulites consisting of conventional smooth lamellae (i.e. without cross-hatch) develop through the familiar sheaving mechanism, as apparent from *Figure 8a*. The resulting spherulites are clearly of category 2. When cross-hatching is present, as in most α-spherulites, then even in the absence of a nucleating foreign particle the growth will be multidirectional. It is expected that the initial crystal will be a trellis structure of mutually orthogonal lamellae (such as can be observed in isolation from solution, the so called 'quadrites'). Here the continuing growth of the lamellae constituting the trellis structure, combined with some fanning and branching, will lead to a spherulite which conforms more closely to category 1, (revealed by *Figure 10*). In other materials spherulites in this class have been considered as a coincidental consequence of the nucleating influence of heterogeneities. We see that in the case of iPP this mode of

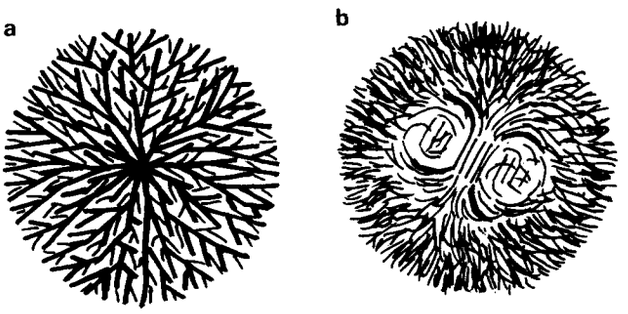

Figure 16 Sketch of two possible growth mechanisms leading to spherical symmetry. (a) central multidirectional growth (category 1), (b) sheaf-like unidirectional growth (category 2)

spherulite growth and the resulting architecture is nevertheless intrinsic to the most frequent form of crystal texture itself.

Lamellae and crystal lattice

The electron diffraction (ED) results are especially noteworthy. Technically, this is the first time that the permanganic etching replication technique could be combined with ED with any polymer. In addition, ED on iPP in any form is notoriously difficult owing to its beam sensitivity.

As already stated above, the observations revealed that the detachment process itself is selective. It extracts lamellae predominantly in the flat-on orientation which implies that the basal, hence fold surface, adheres more strongly to the replicating agent than the lateral surface. This finding in itself may well be of significance for wider ranging issues, such as the nature and surface free energies of the different surfaces and ought to be relevant to the macroscopic phenomenon of adhesion. For the purposes of the present study it has the consequence that most of the diffraction effects observed correspond to the *c* axis view, hence reveal predominantly *hk*0 reflexions (*Figures 12* and *13*). This orientational selectivity is the source of a further type of selectivity for the spherulites with a cross hatched structure. As in a diametral section or thin film spherulite the R component of the cross-hatch exists both in the flat-on and in the edge-on view, while the T component only in the edge-on view, it follows that the extracted lamellae will be predominantly of the R type. Thus we are actually separating the R from the T lamellae.

In spite of the above, some lamellae or portions thereof can be detached in their edge-on projection from samples or regions where this edge-on orientation is the only one present. This is always the situation in highly off-diametral sections (*Figure 11*) but it can apply to appropriate regions of near diametral sections (*Figure 14*).

Electron diffraction patterns obtained in the above manner have two kinds of information to convey. First, they serve to identify the crystal structure within an electronmicroscopic area. This provides further confirmation of spherulite type at least as far as whether it is of the α or β category. Further, it aids correlation of electronmicroscopy with structure information on the bulk (X-ray diffraction), and finally helps to settle issues such as rely on the role of the different crystal structures in the morphology (see reference to γ structure made earlier).

The second function of electron diffraction is to provide information on the relation of crystal orientation with respect to the spherulite, hence crystal growth direction. Accordingly in the α-spherulites the radial orientation of the R lamellae is a^*, which correspondingly is also the crystallographic growth direction of the spherulite irrespective of whether cross-hatching is present or not (*Figure 12*). For the hexagonal β-phase structures the radial growth is along the <300> crystallographic direction (*Figure 14*).

CONCLUSION

The present work has revealed some specific correlations between the structural entities on the different levels of the structure hierarchy. Whilst the overall situation remains intrinsically complex due to the large variety of morphologies iPP displays, at least some system has emerged, which, descriptive as it may be, points toward some unification of so far apparently unconnected phenomena. The most encouraging outcome is the connection and subsequent correlation between the observed optical characteristics and the lamellar microstructures. This includes the recognition that in the α-crystal structure the ratio of the cross-hatch *versus* radial lamellae directly influences the spherulite type, and the clear identification of the β category of spherulites with regular lamellar structures.

It is hoped that this work, revealing the multilevel morphologies by using polarizing optical, electron microscopic and electron diffraction features in a systematic manner, will provide a long outstanding step toward a better understanding of the singularly unusual crystal nucleation and growth behaviour of iPP.

ACKNOWLEDGEMENT

We are greatly indebted to Dr D. J. Blundell for having initiated this work and for his continued interest, instructive advice and for supplying the materials. David Norton wishes to thank the Science and Engineering Research Council and Imperial Chemical Industries PLC, for joint financial support and the latter in particular for placing facilities at our disposal.

REFERENCES

1 Natta, G. and Corradini, P. *Nuovo Cim. Supp.* 1960, **15**, 1
2 Keith, H. D., Padden, F. J., Walter, N. M. and Wycoff, M. W. *J. Appl. Phys.*1959, **30**, 1485
3 Turner-Jones, A., Aizlewood, J. M. and Beckett, D. R. *Makromol. Chem.*1964, **75**, 134
4 Turner-Jones, A. and Cobbold, A. J. *J. Polym. Sci.* 1968, **6**, 539
5 Samuels, R. J. and Yee, R. Y. *J. Polym. Sci. A-2* 1972, **10**, 385
6 Morrow, D. R. and Newman, B. A. *J. Appl. Phys.* 1968, **39**, 4944
7 Kardos, J. L., Christiansen, A. W. and Baer, E. *J. Polym. Sci. A-2*, 1966, **4**, 777
8 Sauer, J. A. and Pae, K. D. *J. Appl. Phys.*, 1968, **30**, 4950
9 Addinck, E. J. and Beintema, J. *Polymer* 1961, **2**, 185
10 Padden, F. J. and Keith, H. D. *J. Appl. Phys.* 1973, **44**, 1217
11 Padden, F. J. and Keith, H. D. *J. Appl. Phys.* 1959, **30**, 1479
12 Binsbergen, F. L. and DeLange, B. G. M. *Polymer* 1968, **9**, 23
13 Lovinger, A. J., Chua, J. O. and Gryte, C. C. *J. Polym. Sci. Polym. Phys. Edn.* 1977, **15**, 641
14 Sauer, J. A., Morrow, D. R. and Richardson, S. C. *J. Appl. Phys.* 1965, **36**, 3017
15 Khoury, F. *J. Res. Natl. Bur. Stand.* 1966, **A70**, 29
16 Geil, P. M. 'Polymer Single Crystals', Interscience, New York, 1963, p 211
17 Padden, F. J. and Keith, H. D. *J. Appl. Phys.* 1966, **37**, 4013
18 Lovinger, A. J. *J. Polym. Sci., Polym. Phys. Edn.* 1983, **21**, 97
19 Olley, R. M., Hodge, A. M. and Bassett, D. C. *J. Polym. Sci., Polym. Phys. Edn.* 1979, **17**, 627
20 Bassett, D. C., Hodge, A. M. and Olley, R. M. *Proc. Roy. Soc.* 1981, **A377**; I, 25: II, 39: III, 61
21 Norton, D. R. *Ph.D. Thesis* 1984, Bristol University
22 Bassett, D. C. 'Principles of Polymer Morphology', Cambridge University Press, 1981
23 Olley, R. M. and Bassett, D. C. *Polymer* 1982, **23**, 1707
24 Norton, D. R. and Keller, A. *J. Mater Sci.* 1984, **19**, 447
25 Norton, D. R. *M.Sc. Thesis* 1981, Bristol University
26 Keedy, D. A., Powers, J. and Stein, R. S. *J. Appl. Phys.* 1960, **31**, 1911
27 Schael, G. W. *J. Appl. Polym. Sci.* 1968, **12**, 903
28 Takahara, H., Kawai, H. and Yamada, T. *Sen-i Gahkaishi* 1967, **23**, 102
29 Wilchinsky, Z. W. North-Jersey Sec. Am. Chem. Soc. Meeting, 1959, taken from ref. 27
30 Clark, E. S. and Spruiell, J. E. *Polym. Eng. Sci.* 1976, **16**, 176